The Astrophysical Journal Letters, 717:L159–L163, 2010 July 10 doi:10.1088/2041-8205/717/2/L159

CORONAL MASS EJECTION PROPAGATION AND EXPANSION IN THREE-DIMENSIONAL SPACE IN THE HELIOSPHERE BASED ON *STEREO*/SECCHI OBSERVATIONS

Watanachak Poomvises, Jie Zhang, and Oscar Olmedo
Department of Computational and Data Sciences, George Mason University, 4400 University Drive, Fairfax, VA 22030, USA
Received 2010 March 29; accepted 2010 June 11; published 2010 June 24

ABSTRACT

We report on several new findings regarding the kinematic and morphological evolution of coronal mass ejections (CMEs) in the inner heliosphere using the unprecedented *STEREO*/SECCHI observations. The CME tracking is based on the three-dimensional Raytrace model, which is free of the projection effect, resulting in true CME velocities. We also measure the cross section size of the CME and hence its expansion velocity. For the four major CME events investigated, we find that their leading edge (LE) velocity converges from an initial range between 400 km s^{-1} and 1500 km s^{-1} at 5–10 $R_\odot$ to a narrow range between 500 km s^{-1} and 750 km s^{-1} at 50 $R_\odot$. The expansion velocity is also found to converge into a narrow range between 75 km s^{-1} and 175 km s^{-1}. Both LE and expansion velocities are nearly constant after 50 $R_\odot$. We further find that the acceleration of CMEs in the inner heliosphere from ∼10 to 90 $R_\odot$ can be described by an exponential function, with an initial value as large as ∼−80 m s^{-2} but exponentially decreasing to almost zero (more precisely, less than ±5 m s^{-2} considering the uncertainty of measurements). These results provide important observational constraints on understanding CME dynamics in interplanetary space.

Key words: Sun: coronal mass ejections (CMEs)

Online-only material: color figures

1. INTRODUCTION

Coronal mass ejections (CMEs) on the Sun are the largest energy release process in the solar system and act as the primary driver of geomagnetic storms and other space weather phenomena on the Earth (e.g., Gosling 1993; Webb et al. 2000; Zhang et al. 2007). The Large Angle and Spectrometric Coronagraph (Brueckner et al. 1995) on board the *Solar and Heliospheric Observatory* satellite located at L1 vantage point is able to detect CMEs and observe their propagation over a large distance. These white light coronagraphs, as any other remote sensing instruments suited at a single point, provide observations only projected on the plane of the sky. However, using the coronagraphs onboard the *Solar Terrestrial Relations Observatory* (*STEREO*; Kaiser et al. 2008) satellites can address the projection effect. *STEREO* is composed of two identical satellites that orbit the Sun on approximately the same orbit as the Earth where one satellite is ahead (A) and the other is behind (B) the Earth. From two vantage points, the *STEREO* coronagraphs are able to measure the true propagation of CMEs in three dimensions through interplanetary space, free of the projection effect (Thernisien et al. 2006, 2009; Liu et al. 2010).

In this study, we examine both the kinematic and the morphological evolution of CMEs in interplanetary space using observations made by *STEREO*. The three-dimensional Raytrace model, developed by Thernisien et al. (2006, 2009), is used as a tool to model and measure the radial propagation of CMEs free of the projection effect. We carefully examined four major events that occurred in 2008 (note that not many major events occur during the solar minimum) that were clearly observed by the COR2 (Coronagraph 2) and HI1 (Heliospheric Imager I) instruments in the SECCHI (Sun Earth Connection Coronal and Heliospheric Investigation) suite. The EUVI (Extreme ultraviolet imager, also part of the SECCHI suite) is used to locate the exact source location of CMEs on the solar surface. We calculate both the leading edge (LE) velocity and the expansion velocity. The bulk propagation velocity is then found from the difference of these two velocities. CME accelerations in the interplanetary space are further derived. In the next section, the measurement technique is described, and the fitting methods of velocity and acceleration are presented. A brief description of the four events is given in Section 3. The results and findings are presented in Section 4. The results are discussed in Section 5.

2. 3D MEASUREMENT AND VELOCITY–ACCELERATION FITTING

The Raytrace model by Thernisien et al. (2006, 2009) represents a CME as a three-dimensional flux rope-like structure, dubbed as a "croissant" model. The geometry of this model splits into two parts: the upper portion as a tubular semi-circle that represents the main body and the lower portion as two cone-shaped legs. This model has six free parameters: Carrington longitude (ϕ) and latitude (θ) of the source region (SR), height or LE of CME (r) along the central axis that joins the Sun center and the LE, tilt angle (γ), half-angle (α) between the two legs anchored on the surface, and the aspect ratio (κ) of the flux rope. The aspect ratio scales the minor radius w (or cross section) of the flux rope with the LE distance:

$$w(r) = \kappa r. \quad (1)$$

The geometry and parameters of the "croissant" model are well illustrated in Figure 1 of Thernisien et al. (2006, 2009). This model can be applied as a tool to make measurements of the propagation of CMEs. This is done by projecting the three-dimensional structure of the model onto the field of view (FOV) of the instruments on-board the two *STEREO* spacecraft. Since the view from the two vantage points will be different, it is possible to constrain the parameters of the model by varying them until the model best approximates the image of the CME as seen in the FOV of the *STEREO* instruments. The resulting structure is then thought to approximate the true

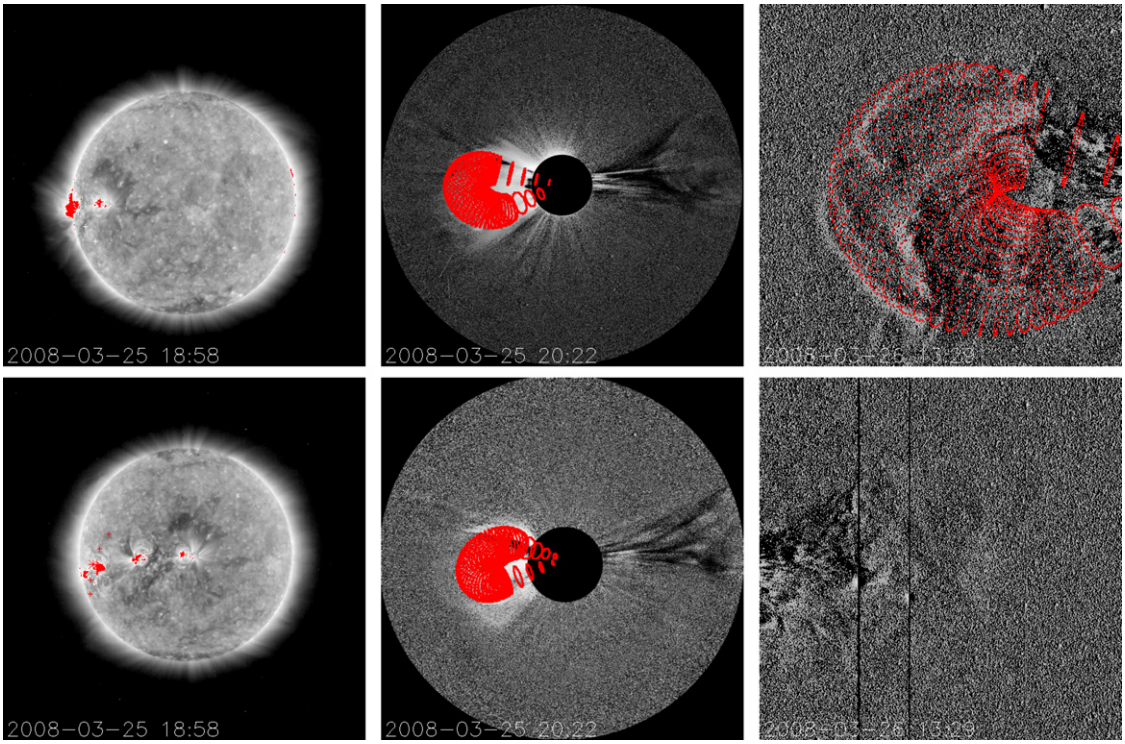

Figure 1. Flux-rope-model measurements (red wire lines) overlaid on the observed images (gray scale) for the 2008 March 25 event. From left to right, the three columns are of EUVI, COR2, and HI1 images, respectively. The top row is for *STEREO A* and the bottom row is for *STEREO B*.
(A color version of this figure is available in the online journal.)

three-dimensional geometrical shape of the CME. By applying this method to a series of images taken simultaneously by *STEREO A* and *B* it is possible to reconstruct the kinematic and morphological evolution of the CME. Figure 1 shows one sample (event on 2008 March 25) of the model measurements overlaid on the observations: EUVI (left column), COR2 (center column), and HI1 (right column); images in the top row are from *STEREO A* observations, while those in the bottom row are from *STEREO B*. EUVI observations are used to locate the CME SR, the preliminary values of longitude and latitude, which are indicated by transient features such as bright flare patches, post-flare loop arcades, and extensive dimming on the disk. In this case, the SR was near the eastern limb in both A and B images. The central location of the SR is indicated by an asterisk symbol (red color in B represents the front-side origin, while white color in A represents the behind-the-limb or backside origin). The footpoints of the CME legs are indicated by plus symbols, while the orientation of these footpoints indicates the tilt angle of the flux rope center axis. The COR2 images (center column) are used to constrain the CME LE, tilt angle, half-angle, and aspect ratio. The appearance of the model is sensitive to the variation of these parameters, in particular, when a pair of images from two perspectives is used to make the constraint simultaneously. The images are further used to fine-tune the longitude and latitude because of the non-radial motion of CMEs in the inner corona. In HI1 (right column), we usually vary only the LE, while keeping all other parameters the same as in the last measurement in COR2. Since the CME on 2008 March 25 was originated on the eastern limb, it appeared in HI1 A images only and was absent in HI1 B, which is expected from the geometric projection.

Three velocities can be derived from above measurements, using the first-order numerical derivative method that is free of assumption of any functional curve (e.g., Zhang et al. 2001). From the height time measurement of the LE, which characterizes the foremost location of the CME in the interplanetary space, the familiar CME LE velocity can be calculated. The CME expansion velocity, which characterizes the cross-section size of the flux rope, is the rate of change of the minor radius. Further, the bulk velocity, which is useful in theoretical modeling of CMEs in terms of overall propagation or translation, is defined as the velocity of the apex (Z) of the axis of the flux rope. Z can be simply inferred from the LE (r) minus the minor radius (w):

$$Z = r - w. \tag{2}$$

Therefore, the LE, bulk, and expansion velocities are calculated from r, Z, and w, respectively:

$$V_L = \frac{dr}{dt}, V_B = \frac{dZ}{dt}, V_E = \frac{dw}{dt}. \tag{3}$$

Further, we find that the LE velocity of the events studied seems to approach an asymptotic value (details will be given in the next section). The velocity profile can be fitted by the following empirical formula:

$$V(r) = V_a + (V_i - V_a)e^{-(\frac{r-r_i}{r_a})}, \tag{4}$$

where V_a is the asymptotic velocity, V_i is the initial velocity at $r = r_i$ (the height of the first data point used in the fitting), and r_a is the e-folding constant from the fitting. Note that the formula fitting starts with the derived velocity profiles, but not the height profiles. This functional form of velocity is a modified version of Sheeley et al. (1999). Our formula is able to describe events that are either decelerating or accelerating to an asymptotic value. If $V_i > V_a$, the event decelerates, and if $V_i < V_a$, the event accelerates. In both cases, the acceleration, or the velocity change rate, goes to approximately zero as r becomes large; in

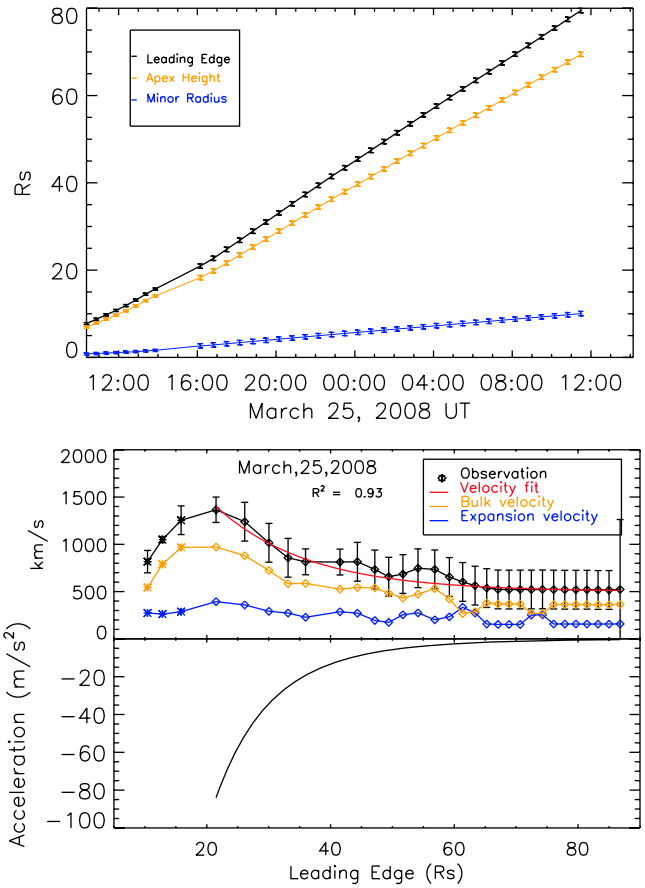

Figure 2. Distance–time (upper panel), velocity–distance (middle panel), and acceleration–distance (lower panel) plots for the CME on 2008 March 25. In the first (second) plot, the three curves—from top to bottom—represent the LE (nominal velocity), the apex (bulk velocity), and the minor radius (expansion velocity), respectively. The red line in the velocity plot shows the functional fitting to the observed LE velocity starting from the peak velocity time. The acceleration curve is derived from the fitted velocity curve. The first three data points are from COR2, and the rest from HI1.

(A color version of this figure is available in the online journal.)

the mean time, the velocity goes to V_a. It is straightforward to derive the acceleration as

$$a(r) = -V(r)\frac{(V_i - V_a)}{r_a}e^{-(\frac{r-r_i}{r_a})}. \quad (5)$$

The effectiveness of the fitting is tested by using the coefficient of determination R^2, which is the square of the sample correlation coefficient between the observed values and their fit values. R^2 will produce values between 0 and 1 depending on how well the empirical formula fits the observation. If the value of R^2 is near 1, the formula fits the observations closely.

3. DESCRIPTION OF EVENTS

Using the methods described above, we have carefully examined four CME events, including both fast and slow events.

3.1. Event: 2008 March 25

The first sign of solar activity for this event was found on the solar disk at 18:00 UT on 2008 March 25 by EUVI A and B at Carrington longitude ∼199° and latitude ∼−11°. The source active region is NOAA AR 0988 with a heliographic coordinate at about S09°E59°. In Figure 2, we show the measurement of the CME's LE, minor radius and apex height with time (top panel) and the derived velocities (middle panel) and acceleration (bottom panel) with distance from the center of the Sun. The first three points in the top and middle panels of Figure 1 are derived from COR2 and the remaining from HI1. The values of uncertainty in the height time plot for LE, minor radius and apex height (top panel) are approximated as 0.12 $R_\odot$ in COR2 and 1.0 $R_\odot$ in HI1 respectively. This uncertainty corresponds to about 8 pixels in both COR2 and HI1 images. We believe that this is a conservative estimation for events with shapes of sharp contrast, but a reasonable one for more diffusive events. Detailed discussions on the sensitivity of model parameters are carried out by Thernisien et al. (2009).

The LE velocity of this event at 20 $R_\odot$ is about 1500 km s^{-1}, then decreases to about 500 km s^{-1} at 65 $R_\odot$. At these two locations, the expansion velocities are about 500 km s^{-1} and 150 km s^{-1}, respectively, while the bulk velocities are about 1000 km s^{-1} and 350 km s^{-1}, respectively. The red line in the middle panel shows the fitted LE velocity using Equation (4). The goodness of fit (R^2) for this event is found to be 0.93, which indicates that the LE velocity fit well matches the observational data obtained by the forwarding model. Moreover, the corresponding acceleration profile (shown in the bottom panel) indicates that the CME is decelerating with an initial rate of about −83.9 m s^{-2} at ∼21.5 $R_\odot$ and then gradually approaches zero.

3.2. Event: 2008 April 26

This event was originated at NOAA AR 0992 with heliographic coordinate N13°W32° and Carrington longitude ∼204° and latitude ∼3°. This CME is a partial halo from the point of view of *STEREO A*. The evolution of the velocities of this CME is shown in Figure 3 (top panel). The LE velocity of this event at 13 $R_\odot$ is about 720 km s^{-1} and the velocity decreases to about 640 km s^{-1} at 40 $R_\odot$ and thereafter. Additionally, the minor radius expansion velocity converges to about 140 km s^{-1} and the bulk velocity to about 500 km s^{-1} at large distances. The initial and final LE velocities that we obtain are consistent with those of previous studies of this event (Thernisien et al. 2009). The goodness of the velocity fitting R^2 for this event is 0.66. The low value is probably due to the fact that, between 20 and 28 $R_\odot$, this event was only seen by HI_1A and had not yet reached the FOV of HI1 B. This means that during the height range 20–28 $R_\odot$, the geometrical fitting had to be done with one vantage point only. Therefore, the uncertainty in the measurement during this height range is expected to be higher than if the geometrical fitting was done with two vantage points.

3.3. Event: 2008 May 17

The active region associated with this event is seen on the northeastern limb by *STEREO A* and close to the center of the solar disk by *STEREO B* on 2008 May 17 at 11:52 UT. It is located at Carrington longitude 261° and latitude 11°. We measured the velocity of this event at 20 $R_\odot$ to be about 1000 km s^{-1}. The velocity then decreased to approximately 720 km s^{-1} after 40 $R_\odot$ and remained approximately constant up to 50 $R_\odot$, where we stopped making measurements. In addition, the value of goodness of fitting for this event is 0.81. This number indicates that the fitting LE velocities are fairly close to the observations. The minor radius expansion velocity and bulk velocity for this event are 150 km s^{-1} and 670 km s^{-1}, respectively, in the region between 40 and 50 $R_\odot$. This result is in close agreement with a previous study done by Wood et al. (2009), who showed that the initial velocity at 6 $R_\odot$ is

Table 1
Geometric and Kinematic Parameters of CMEs in the Inner Heliosphere

Date/Time (YYYYMMDD HH:MM)	ϕ^a (°)	θ^a (°)	γ^a (°)	LE^a ($R_\odot$)	κ^a (°)	α^a	$r_i{}^a$ ($R_\odot$)	$r_a{}^a$ ($R_\odot$)	$V_i{}^a$ (km s^{-1})	$V_a{}^a$ (km s^{-1})	a^b (m s^{-2})
20080325 20:22[c]	199	−12	−44	10	0.20	21	15.0	...	1400.0	...	−83.9
20080326 16:49[d]	199	−5	−44	86	0.30	28	...	21.5	...	500.0	...
20080426 17:22	204	3	−16	13	0.20	12	13.7	...	720	...	−4.0
20080427 08:09	204	−4	−16	79	0.27	23	...	15.0	...	640	...
20080517 11:52	261	−12	−35	10	0.20	15	10.0	...	1000	...	−8.3
20080518 00:49	261	−11	−35	70	0.21	15	...	60.0	...	500	...
20081212 10:22	73	7	87	7	0.10	18	6.0	...	350	...	11.45
20081213 11:49	61	6	87	79	0.12	19	...	9.0	...	590	...

Notes.
[a] The meanings of these parameters are as indicated in the text.
[b] The initial acceleration rate at r_i.
[c] The first time of the CME appearing in COR2 FOV with effective measurement.
[d] The last time of the CME appearing in HI1 FOV with effective measurement.

about 900 km s^{-1} and the final velocity is about 600 km s^{-1} as measured from in situ data at *STEREO B*. One could then come to the conclusion that after the deceleration, which occurred before 40 $R_\odot$, this CME propagated with an almost constant velocity through the interplanetary space up to 1 AU.

3.4. Event: 2008 December 12

This event is considered to be a gradual event because the initial velocity is found to be ∼350 km s^{-1} and the final velocity is about 590 km s^{-1} (Figure 2, bottom panel), indicating a gradual acceleration from a low initial velocity. The SR was at 72° in Carrington longitude and 11° in latitude on 2008 December 12 at 10:22 UT. The minor radius expansion and bulk velocity at about 80 $R_\odot$ were found to be 90 km s^{-1} and 500 km s^{-1}, respectively. This CME manifested as a magnetic cloud in the near-Earth space from in situ measurements (Davis et al. 2009; Liu et al. 2010). The speed of the magnetic cloud is about 350 km s^{-1}, indicating a deceleration of the CME from 80 $R_\odot$ to 1 AU. Nevertheless, this average deceleration is about −1.1 m s^{-2}, which is rather small compared with the acceleration close to the Sun in the COR2 FOV. Therefore, the asymptotic assumption of the fitting is still valid as a good approximation of CME evolution in the inner heliosphere. In addition, we found that the value of goodness of fitting for this event is 0.89.

4. RESULTS

Table 1 summarizes the geometric-fitting parameters (Columns 2–7) and the kinematic-fitting parameters (Columns 8–12) for the four events studied. There are two rows of parameters for each event: the first row indicates the initial parameters at the time when the CME was first observed by COR2, and the second row indicates the final parameters at the time when the CME was last observed by HI1. Except for the LE, the other five geometric parameters of any individual CME in the six-parameter flux-rope model do not change significantly during its evolution in the heliosphere, i.e., from about 10 to 90 $R_\odot$. Nevertheless, there are sometimes noticeable changes in order to best fit the observations. For instance, the heliographic latitude of the apex of the CME on 2008 March 25 gradually moved toward the equator from about S12° to S6°. The heliographic longitude of the gradual CME on 2008 December 12 shifted from 73° to 61°. The angular width of CMEs on 2008 March

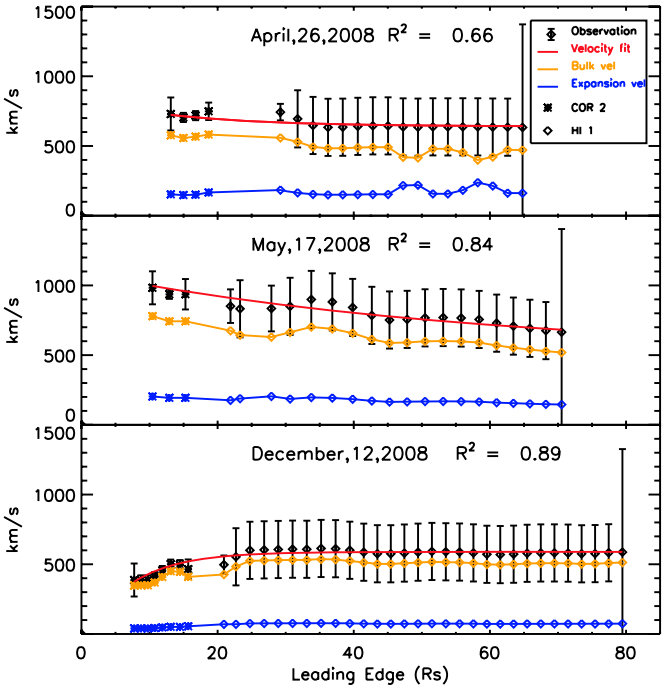

Figure 3. Velocity–distance profiles for three CMEs (in the three panels, respectively). In each panel, the three curves from top to bottom represent the LE velocity, bulk velocity, and expansion velocity, respectively. The red line shows the functional fitting to the observed LE velocity. Error bars are only shown for the LE velocity, and they are similar for the other two velocities (not shown to avoid clutter).
(A color version of this figure is available in the online journal.)

25 and 2008 April 26 also increased by more than 10° when they traveled across the COR2 and HI1 FOVs. While there are uncertainties associated with the model fitting (see Thernisien et al. 2009 for details), we believe that these changes are larger than the fitting errors and thus are true changes of CMEs. The variations (and the fitting errors) of these parameters are not the purpose of this Letter, and therefore we will not discuss them further. Also note that our results are generally in agreement with that of Thernisien et al. (2009) which are based on COR2 data only. We now focus on the kinematic evolution of the CMEs studied.

We show in Figure 4 the composite plots of the fitted velocity profiles (upper panel) and the acceleration profiles of the four

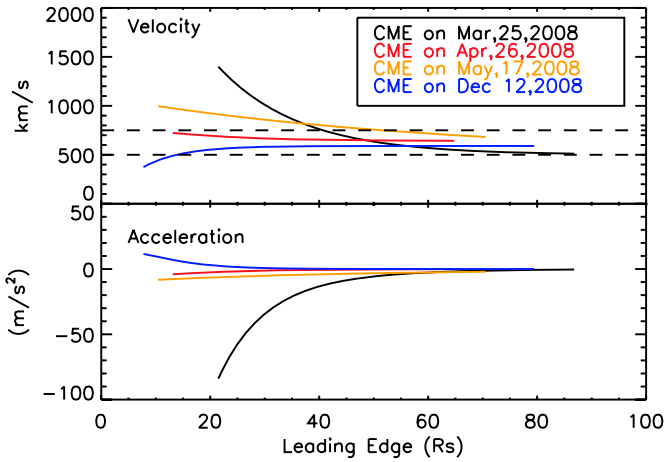

Figure 4. Fitted velocity profiles (top panel) and acceleration profiles (bottom panel) for the four events studied. These profiles are described by an exponential function approaching an asymptotic value with distance. Note that the velocities and accelerations quickly converge toward a narrow range as CMEs move out.
(A color version of this figure is available in the online journal.)

CMEs studied. It can be seen that the LE velocities converge to a narrow range between 500 and 750 km s^{-1} after about 50 $R_\odot$, even though the beginning velocities of these CMEs have a much larger range from 350 km s^{-1} to 1500 km s^{-1}. For any individual CMEs, the velocity is almost constant after 50 $R_\odot$; the change is too small to be appreciated by the method employed in this Letter. This observation justifies the choice of the velocity function to be exponential, in order to quickly converge into an asymptotic value.

Further, the rate of change of the velocity, the acceleration, is far from constant with distance (Figure 4, lower panel). The acceleration function is also exponential, because of the choice of the velocity function. As seen in the figure, the acceleration profiles decrease to a very small value after 50 $R_\odot$, as small as $\pm$ 5 m s^{-2}. The acceleration (or deceleration for a fast CME) is much stronger when it is close to the Sun. The initial acceleration of the 2008 March 25 CME has a value of -83.9 m s^{-2} when the CME is at 15 $R_\odot$. This value is -8.3 m s^{-2} for the 2008 May 17 event. For the gradual and slow CME on 2008 December 12, the initial acceleration is +11.5 m s^{-2} at about 8 $R_\odot$. On the other hand, the 2008 April 26 CME shows very small acceleration in the entire FOV studied: the acceleration is only -4.0 m s^{-2} at the distance of 13 $R_\odot$ from the Sun.

Another interesting result is that the expansion velocity is largely proportional to the LE velocity (Figure 3). This is true for both the decelerating fast events and the accelerating slow events. When the LE velocity decreases, the expansion velocity decreases. Similarly, when the LE velocity increases, the expansion velocity also increases. The parameter of the aspect ratio (κ) measured in the geometric model (Column 6 in Table 1) is equal to the ratio between the expansion velocity and the LE velocity. For the three fast events studied, the ratio is between 0.2 and 0.3, indicating that the LE velocity is about three to five times larger than the expansion velocity. For the gradual and slow event, the expansion velocity is about 10 times smaller than the LE velocity. Further, the expansion velocity may become relatively smaller compared to the LE velocity as the distance from the Sun increases, since the aspect ratio seems to increase with the distance (nevertheless, the study of the quantitative change of the aspect ratio with distance is difficult, because of the limited accuracy of the measurement).

5. DISCUSSIONS

There are several new findings in this Letter. First, the LE velocity of CMEs converges rather quickly in interplanetary space, e.g., from an initial range between 400 km s^{-1} and 1500 km s^{-1} at 5–10 $R_\odot$ to a narrow range between 500 km s^{-1} and 750 km s^{-1} at about 50 $R_\odot$. Expansion velocities are also found to converge into a narrow range between 75 km s^{-1} and 175 km s^{-1}. Second, both LE and expansion velocities for any individual CMEs are nearly constant after 50 $R_\odot$. Third, the acceleration of CMEs in the inner heliosphere from $\sim$10 to 90 $R_\odot$ can be modeled by an exponential function. Fitting the LE velocity to an exponential function has been done before (Sheeley et al. 1999). However, we show in this Letter that this functional form is valid for a large distance in interplanetary space.

It seems that the kinematic evolution profile in the inner heliosphere is probably attributed to the drag force between the CME and the ambient solar wind. The observed initial deceleration for fast events, which is on the order of tens of m s^{-2}, cannot be explained by the gravitational force and the slow-down effect of mass pile-up in front of CMEs (Sheeley et al. 1999). The solar wind drag force is proportional to the square of the velocity difference between the CME and the solar wind (e.g., Chen 1996; Cargill 2004). Therefore, the acceleration is the largest when the velocity difference is the largest, and goes to almost zero when the two velocities are close to each other. The asymptotic value of the CME velocity seems to be constrained by the ambient solar wind speed.

The close correlation between the expansion velocity and the LE velocity of individual CMEs indicates that, to the first order of approximation, the CME evolution can be treated as a self-similar expansion superposed on the bulk outward motion, The expansion contributes a non-trivial component to the overall velocity at the LE, e.g., 30% for fast events and 10% for slow events. It is likely that this expansion is driven by the CME internal thermal pressure overcoming the ambient solar wind pressure (Wang et al. 2009). A detailed theoretical study of the CME expansion, as well as the bulk propagation in the inner heliosphere, will be pursued in a separate paper.

This research is supported by grants from NASA NNG07AO72G and NSF ATM-0748003. The authors acknowledge many valuable discussions with A. Thernisien.

REFERENCES

Brueckner, G. E., et al. 1995, Sol. Phys., 162, 357
Cagill, P. 2004, Sol. Phys., 221, 135
Chen, J. 1996, J. Geophys. Res., 101, 27499
Davis, C. J., Davies, J. A., Lockwood, M., Rouillard, A. P., Eyles, C. J., & Harrison, R. A. 2009, Geophys. Res. Lett., 36, L08102
Gosling, J. T. 1993, J. Geophys. Res., 98, 18937
Kaiser, M. L., Kucera, T. A., Davila, J. M., St. Cyr, O. C., Guhathakurta, M., & Christian, E. 2008, Space Sci. Rev., 136, 5
Liu, Y., Davies, A. J., Luhmann, J., Vourlidas, A., Bale, D. S., & Lin, R. 2010, ApJ, 710, L82
Sheeley, N. R., Jr., Walters, J. H., Wang, Y. M., & Howard, R. A. 1999, J. Geophys. Res., 104, 24739
Thernisien, A., Howard, R. A., & Vourlidas, A. 2006, ApJ, 652, 763
Thernisien, A., Vourlidas, A., & Howard, R. A. 2009, Sol. Phys., 256, 111
Wang, Y., Zhang, J., & Shen, C. 2009, J. Geophys. Res., 114, A10104
Webb, D. F., Cliver, E. W., Crooker, N. U., Cry, O. C. S., & Thompson, B. J. 2000, J. Geophys. Res., 105, 7491
Wood, B. E., Howard, R. A., Thernisien, A., Plunkett, S. P., & Socker, D. G. 2009, Sol. Phys., 259, 163
Zhang, J., Dere, K. P., Howard, R. A., Kundu, M. R., & White, S. M. 2001, ApJ, 559, 452
Zhang, J., et al. 2007, J. Geophys. Res., 112, A12103